USGS
science for a changing world

Studies by the U.S. Geological Survey in Alaska, 2007

Quaternary Uplift History of Wingham Island, South-Central Alaska

Professional Paper 1760–B

U.S. Department of the Interior
U.S. Geological Survey

This page intentionally left blank

Studies by the U.S. Geological Survey in Alaska, 2007

Quaternary Uplift History of Wingham Island, South-Central Alaska

By James B. Chapman, Peter J. Haeussler, and Terry L. Pavlis

Professional Paper 1760–B

U.S. Department of the Interior
U.S. Geological Survey

U.S. Department of the Interior
KEN SALAZAR, Secretary

U.S. Geological Survey
Suzette M. Kimball, Director

U.S. Geological Survey, Reston, Virginia: 2009

This report and any updates to it are available online at:
http://pubs.usgs.gov/1760/b/

For more information about the USGS and its products:
Telephone: 1–888–ASK–USGS (1-888-275-8747)
World Wide Web: http://www.usgs.gov/

Produced in the Western Region, Menlo Park, California
Manuscript approved for publication, February 18, 2009
Text edited by Tracey Suzuki
Layout and design by Stephen L. Scott

Suggested citation:
Chapman, J.B., Haeussler, P.J., and Pavlis, T.L., 2009, Quaternary uplift history of Wingham Island, south-central Alaska, *in* Haeussler, P.J., and Galloway, J.P., eds., Studies by the U.S. Geological Survey in Alaska, 2007: U.S. Geological Survey Professional Paper 1760-B, 13 p. [http://pubs.usgs.gov/1760/b/].

FRONT COVER
Photograph of Wingham Island taken from Suckling Hills looking west-southwest. (Photograph by James B. Chapman.)

Contents

Figures

Tables

This page intentionally left blank

Studies by the U.S. Geological Survey in Alaska, 2007
Edited by Peter J. Haeussler and John P. Galloway
U.S. Geological Survey Professional Paper 1760–B

Quaternary Uplift History of Wingham Island, South-Central Alaska

By James B. Chapman[1], Peter J. Haeussler[2], Terry L. Pavlis[1]

Abstract

Marine terraces cut into Pleistocene deposits on Wingham Island in the Gulf of Alaska provide new constraints on the position of sea level, ice thickness and total glacioisostatic rebound at the end of the Last Glacial Maximum. A radiocarbon age of 13.9 ± 0.15 ka on the most prominent terrace is coincident with the end of meltwater pulse 1A, possibly suggestive of a link between changes in relative sea level and terrace formation. Isostatic modeling suggests a local ice thickness of 600 to 700 m with high (~10 cm/yr) initial rates of postglacial rebound. In addition to the unique ties to meltwater pulse 1A, the timing of emergence for Wingham Island following the Last Glacial Maximum has implications for the early migration of humans into North America.

Introduction

The coastal St. Elias Mountains in southern Alaska contain the largest glaciers and most extensive ice fields on the North American continent. However, the glacial extent and timing of retreat following the Last Glacial Maximum (LGM) are poorly constrained (Hamilton, 1994; Kaufman and Manley, 2004). Additionally, the sea-level response and isostatic effect from collapse of these glacial systems at the end of the LGM are relatively unexplored.

In this paper, we describe unconsolidated sedimentary deposits at Wingham Island of probable Pleistocene age, into which are cut a series of marine terraces. New radiocarbon ages suggest a temporal correlation between incision of the highest terrace and meltwater pulse 1A (MWP1A), characterized by rapid eustatic sea level rise. We apply two models of glacioisostatic rebound to compare local uplift with eustatic sea-level in order to asses whether terrace incision at Wingham Island is compatible with a lull in relative sea-level (RSL) fall during MWP1A. We also provide new estimates of ice thickness and total isostatic uplift and comment on local rates of ice retreat. Finally, we speculate on the relationship between the timing of glacial retreat, paleogeography, and early human migration into the Americas by means of a coastal route.

Geologic Setting

Wingham Island is located at the easternmost extent of the Aleutian subduction zone, along the edge of the Yakutat microplate, which is presently being subducted beneath North America (fig. 1). A local splay-fault system on the Aleutian megathrust, the Kayak Island Zone (Plafker and others, 1994), surfaces 10 to 15 km southeast of Wingham Island and is currently uplifting Kayak Island and the Suckling Hills (fig. 1). Tilting of an upland surface in the Suckling Hills (Chapman and Vorkink, 2006) and backlimb rotation within the Kayak Island Zone, as imaged in a high-resolution seismic line (Worthington and others, 2008), suggest that significant tectonic uplift occurred since the LGM. This deformation is highly concentrated near the Kayak Island zone and drops to undetectable levels 5 to 10 km to the northwest. The entire region is uplifted during megathrust events, including 1 to 3 m of uplift during the last event in 1964 (Plafker, 1969), but paleoseismic studies suggest that coseismic slip is recovered within a few centuries (Shennan and others, 1999), well within the proposed 500 to 900 yr recurrence interval (Cohen and Freymueller, 2005; Hamilton and Shennan, 2005a, 2005b). On the basis of these studies, we make the simplifying assumption that nearly complete interseismic relaxation occurs before the next earthquake, such that Wingham Island has experienced negligible net vertical tectonic uplift (<5 m) since the LGM.

The majority of Wingham Island is surrounded by steep sea cliffs cut into Tertiary sedimentary and volcanic rocks of the Orca Group, part of the Cenozoic accretionary complex rimming southern Alaska (Plafker and others, 1994). At the southern tip of the island, the Orca Group is thrust over sedimentary rocks of the Yakutat microplate, locally forming a suture zone (fig. 2). Sedimentary units consist of syntectonic glaciomarine mudstones and diamicts of the Pliocene and

[1]Department of Geological Sciences, Geology 405, 500 West University Boulevard, Univeristy of Texas at El Paso, El Paso, TX 79968.
[2]U.S. Geological Survey, 4200 University Drive, Anchorage, AK 99508.

younger Yakataga Fm. (Eyles and others, 1991); marine shales and siltstones of the ~Oligocene Poul Creek Fm. (Plafker, 1987); and shallow marine sandstones of the Redwood Fm. (K. Ridgway, oral comm., July 2007), which is laterally equivalent with the basal Yakataga Fm. (Plafker and others, 1987). There is a large topographic escarpment (~80 m) at the boundary between the Redwood Fm. and Poul Creek Fm. that likely records an erosional event that preferentially eroded the friable shales within the Poul Creek Fm. Buttressed against this bedrock escarpment are up to 55 m of unconsolidated marine to terrestrial deposits (fig. 3*A*), previously estimated to be Quaternary in age (Miller, 1961; Plafker, 1974). The deposits are sheltered within a small cove and are protected from the direction of the Pacific storm track by Kayak Island (figs. 1 and 2), which may explain their preservation.

Associated with these deposits are four terraces (t_3–t_0, fig. 2). Terrace t_3 is a depositional terrace at ~40 m above mean sea level that gently slopes to the south of the island and is cut into by erosional terrace t_2 at ~20 m. Terrace t_1 consists of beach and dune deposits uplifted ~ 2 m during the 1964 Alaska earthquake (Plafker, 1969). We mapped the upper limit of t_1 by using an aerial photograph taken in 1952 (fig. 2). The 1964 Alaska earthquake also exposed terrace t_0, a marine terrace cut into bedrock that was uplifted into the intertidal zone (figs. 3*A* and *B*; Plafker, 1969). Because coseismic slip is recovered, t_0 was likely formed during several earthquake cycles.

Glacial History

During the LGM, glacial systems within the St. Elias Mountains were part of the Cordilleran Ice Sheet that stretched from central Alaska to Puget Sound and abutted the Laurentide Ice Sheet to the east (Clague and James, 2002; Booth and

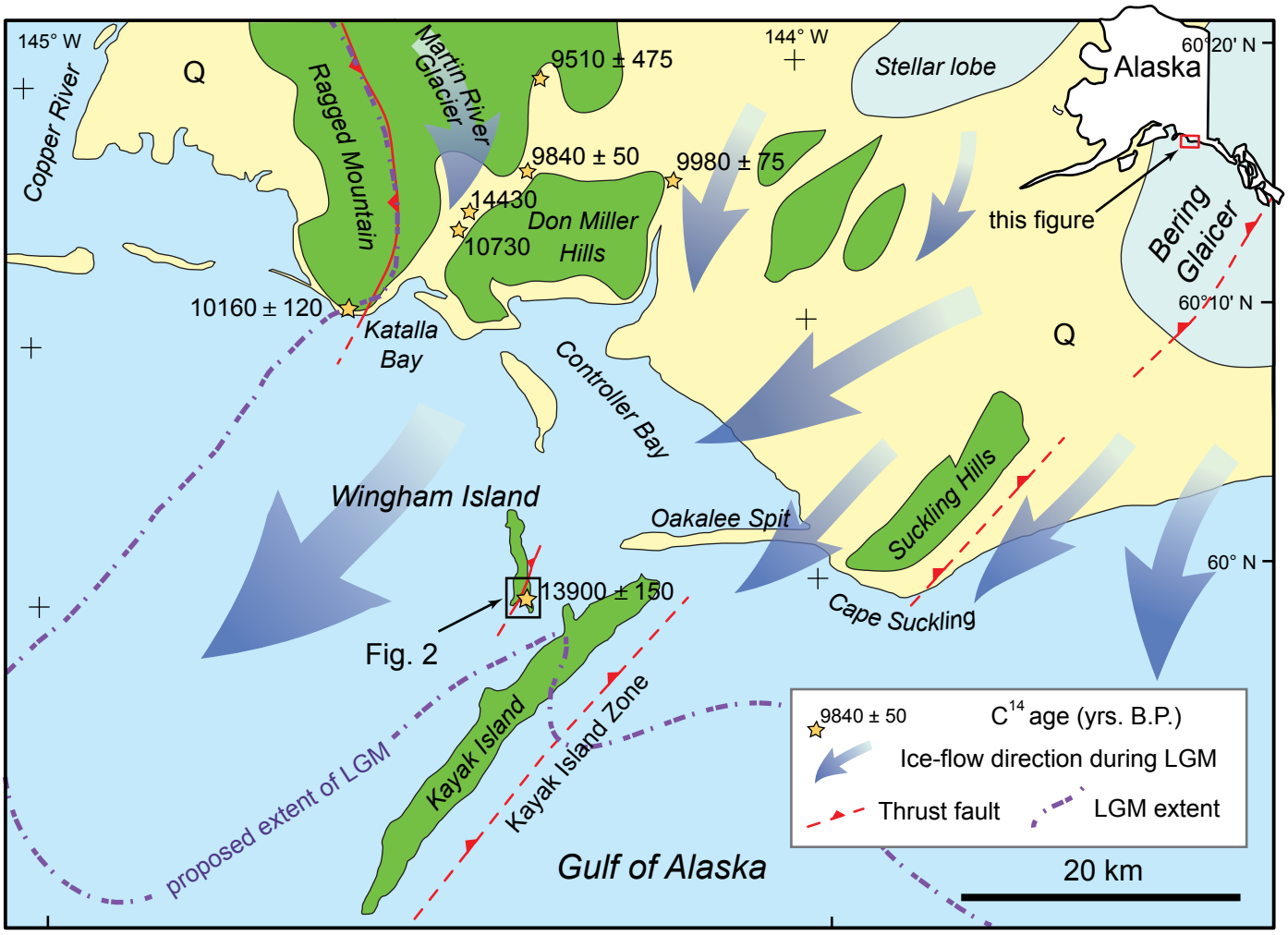

Figure 1. Overview map of the Wingham Island area showing major faults, proposed glacial extent during the Last Glacial Maximum (LGM), and ice flow direction of major glaciers. Orange stars are radiocarbon dates that represent minimum ages for glacial retreat as reported in Huesser (1960), Sirkin and Tuthill (1987), Fleisher and others (1999), and this study. All ages were calibrated to calendar years B.P. Q, Quaternary sediments.

others, 2004). The glacial history of the St. Elias Mountains remains one of the least well-defined in the Cordillera due to poor exposure and a lack of preservation of glacial geomorphic features (Hamilton, 1994). Early workers in the area believed that many glaciers, including the Bering and Martin River glaciers were never more extensive than their present position (Miller, 1958; Reid, 1970), but evidence has since accumulated that documents large glacial advances in the LGM. Maximum extent is constrained by bathymetric surveys of sea valleys (Carlson and others, 1990; Muller and Fleisher, 1995; Green and others, 2007) and glacial erratics or till deposits at Cape Suckling, the entrance to Katalla Bay near the Don Miller Hills, and the southern tip of Ragged Mountain (fig. 1) (Fleisher and others, 1999; Muller and Fleisher, 1995). We slightly expanded the maximum glacial extent of Kaufman and Manley (2004) to reflect what we interpret as glacially influenced topography on Wingham and Kayak Islands and large (3-5 m diameter) glacial erratics on terrace t_0, although they may also be ice-rafted dropstones (fig. 3*B*). Fleisher and others (1999) identified Quaternary deposits at 165 m elevation on the flanks of the Suckling Hills that they interpreted as glacially dammed lacustrine sediment, suggesting a minimum ice thickness of ~165 m, although tectonic uplift has not been considered; the deposits may be related to a post-LGM advance. No other published estimates of ice thickness exist for this area.

The glacial maximum and beginning of ice retreat for the Cordilleran Ice Sheet (14-16 ka) lagged a few thousand years behind that of the Laurentide Ice Sheet (18-20 ka; Clague and James, 2002). Mann and Hamilton (1995) suggest the glacial complex in Cook Inlet broke up prior to 16.5 to 16 ka, and deglaciation was underway by 14.5 ka on the Kenai Peninsula (Rymer and Sims, 1982), by 16 to 15 ka in the Queen Charlotte Islands (Blaise and others, 1990), before 13.7 ka just west of Icy Bay (Denton, 1974), and as early as 14.5 ka in the Katalla Bay area (Sirkin and Tuthill, 1987). Fleisher and others (1999) report younger (~10 ka) ages for basal peat layers overlying till deposits in the Katalla area (fig. 1), although those ages may represent a significant delay in peat formation (Gorham and others, 2007), or post-

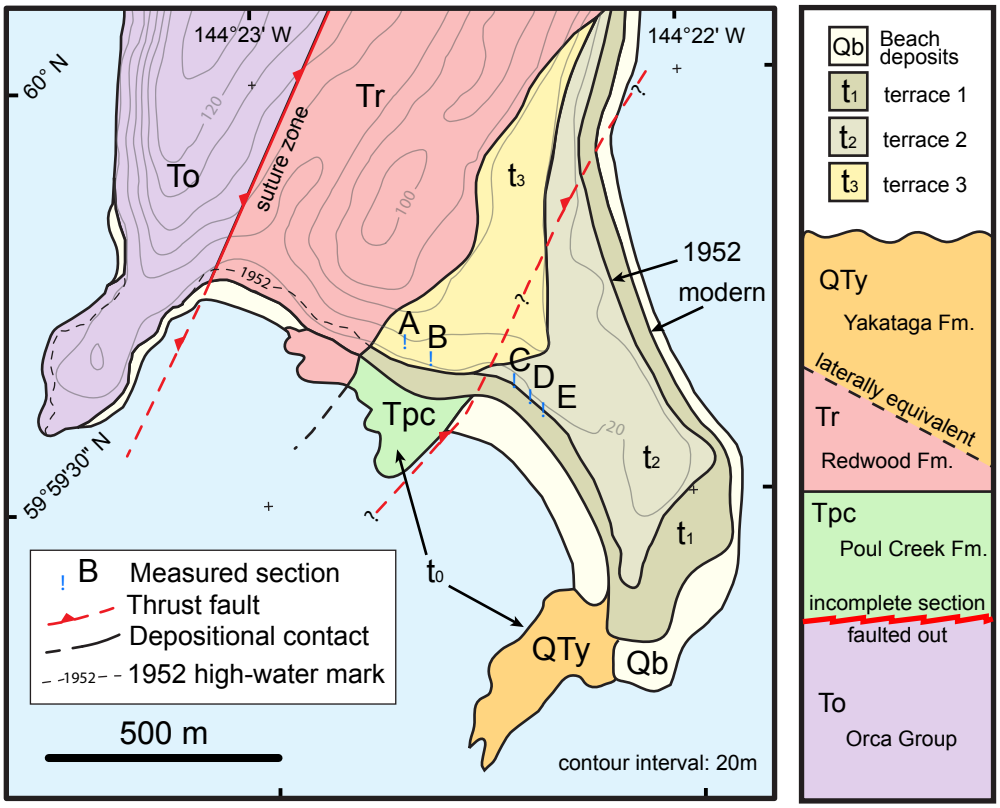

Figure 2. Geologic map of southern Wingham Island showing bedrock and surficial units, modified from Plafker (1974). Terrace t_3 is a depositional terrace that forms a buttress unconformity against a bedrock escarpment. Terraces t_2 and t_1 are incised into the deposits of t_3 and terrace t_0 is a bedrock strath terrace. The upper extent of t_1 was mapped using an aerial photograph taken in 1952. The position of the thrust fault between sections B and C is uncertain and could occur anywhere within the small cove.

Figure 3. Photographs from Wingham Island. *A*, A northeast looking aerial view of the buttress unconformity and unconsolidated deposits. *B,* The largest glacial erratic or dropstone found on terrace t_0. C-G from section B, and H from section D. *C*, Granular conglomerate and shell hash within unit 1 and a small reverse fault oriented 019/57 (strike dip following right-hand rule). *D*, Alternating silt and sand layers in unit 2. *E*, Low amplitude, long wavelength cross-stratification in unit 3. P. Haeussler for scale is pointing at silt rip-up clasts at the base of the unit. *F*, J. Chapman for scale is pointing at a mud-drape in unit 3, ~2 m above photograph E. Mud-injections cross-cut unit 3 and in some cases have offset associated with them. *G*, Unit 4 containing prominent peat layers, of which the uppermost was sampled for radiocarbon dating. Unit 5 conformably overlies unit 4. *H*, Fine lamina of heavy minerals on foresets within unit 5.

LGM glacial readvances. Since the LGM, there have been at least two to three ice readvances, including a Younger Dryas event (Muller and Fleisher, 1995). At a minimum, the available data suggests that nearby glaciers had reached their present position by 9.6 to 9.3 ka (Hamilton, 1994). Glaciers may have also retreated well beyond their present position in the early Holocene (7-13 ka) when the terminus of the Bering Glacier was located ~30 km further inland and marine conditions prevailed (Pasch and Foster, 2006; Muller and Fleisher, 1995). Together, these ages provide an incomplete record of ice retreat that our data helps to expand.

Contemporaneous with local ice retreat was eustatic sea-level rise that began ~19.5 ka with the melting of global ice sheets (fig. 4; Lambeck and others, 2002; Lambeck and Chapell, 2001). Total sea-level rise is estimated to be 120 to 135 m (Clark and Mix, 2002) and was punctuated by periods of moderate sea-level rise, like the Younger Dryas, and relatively rapid sea-level rise, like MWP1A (fig. 4; Fairbanks, 1989; Bard and others, 1990; 1996). MWP1A corresponds to a sudden increase in RSL rise around 14 ka, although the exact magnitude and timing is debated. Some researchers suggest a rapid rise (4.5-6 cm/yr) during a short interval (500-1,000 yrs; Blanchon and Shaw, 1995; Bard and others, 1996; Hanebuth and others, 2000) while others prefer more conservative estimates of 1 to 2 cm/yr averaged over much longer periods (~3,500 yrs; Lambeck and others, 2002).

Methods and Results

Stratigraphy

We collected data from Wingham Island for three days during the 2007 field season as part of the St. Elias Erosion and Tectonics Project (STEEP). Quaternary sedimentary deposits first noted by Miller (1961) were surveyed by using a tape measure and linked to extreme high tide (driftwood line) by using a laser range finder. On the basis of repeated measurements and correlation to U.S. Geological Survey (USGS) topographic maps, we estimate a vertical error of <5 m. We examined silt samples (stars in fig. 5) for compositional and biological variation to help determine depositional environment. We sampled for radiocarbon throughout the stratigraphic section and report all ^{14}C ages in calendar years before present.

We divided the deposits into 5 units, which are presented in Sections A-E (figs. 2 and 5). The lowermost unit, unit 1, consists of <5 m of tan to light brown, coarse sand to sub-rounded granular conglomerate with shell hash (fig. 3*C*). Disarticulated shells within the hash are concave down, a hydrodynamically stable position in high-energy depositional environments (Messina and Labarbera, 2004). There are also discontinuous layers of charcoal and woody material, which are beyond the limit of the radiocarbon method (reported as >48 ka, table 1). We interpret unit 1 as a beach-to-surf zone facies. Bedding in unit 1 is oriented 275/04 (strike/dip, following the right-hand rule), roughly consistent with all other units and in the down-dip direction of regional faults and structural grain (fig 2). Small, narrow, thrust faults with offset <30 to 40 cm (fig. 3*C*), are present throughout the measured sections and locally offset layers within the unit. We did not perform an extensive survey of faults within the area, although two fault sets oriented 019/57 and 189/46 appear to be dominant. In most sections, the base of unit 1 is covered by slope wash and mass-wasting deposits, however, in section A, bluish-gray silt to sand beds with scattered shell fragments appear with increasing frequency toward the base of unit 1, suggestive of an unrecognized silt unit older than unit 1.

Unit 1 is separated from unit 2 by a sharp planar contact, parallel to stratification with a significant grain

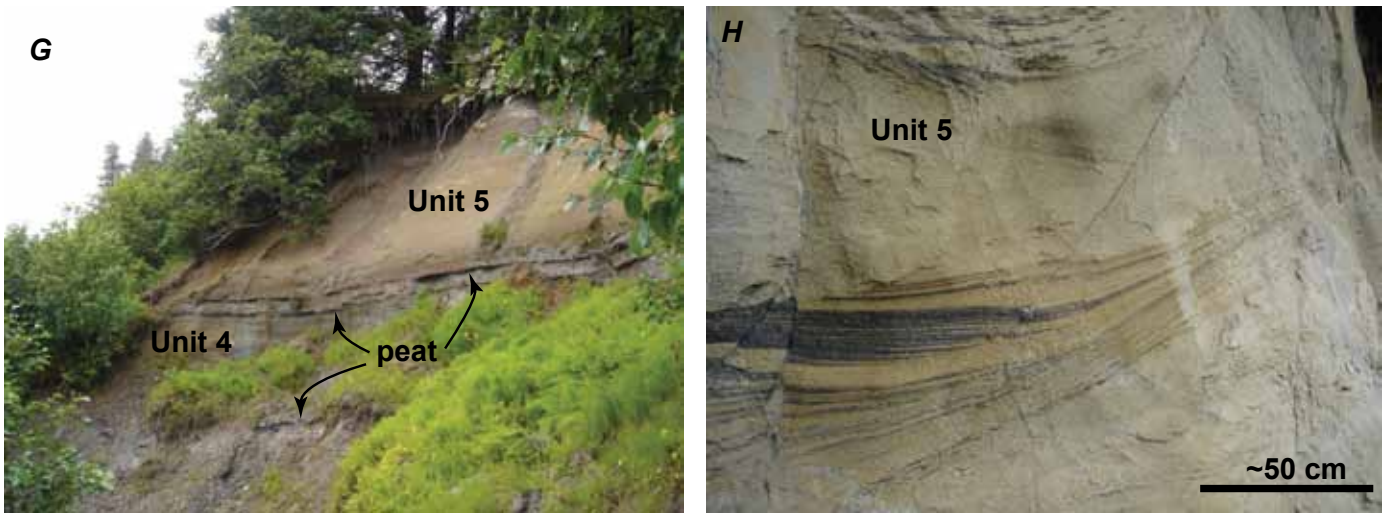

Figure 3. Continued.

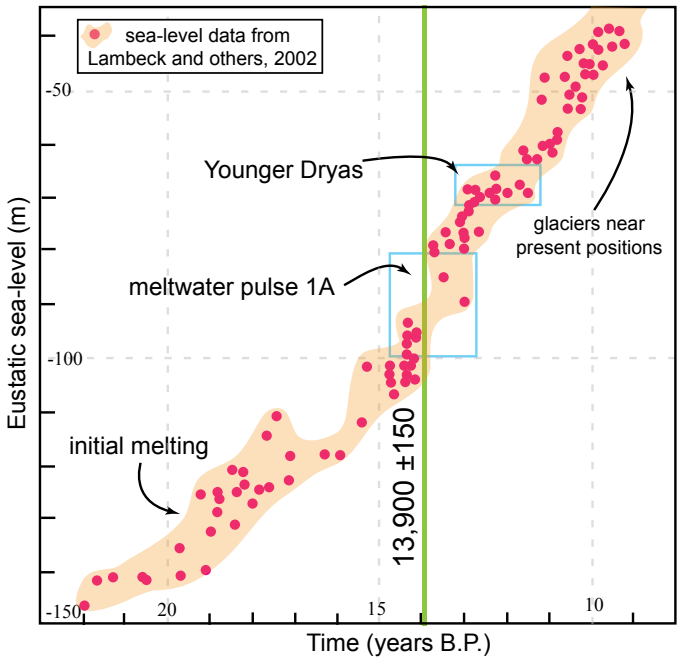

Figure 4. The radiocarbon age from section D (green vertical line) is plotted with eustatic sea-level data (pink dots), in respect to the present, as presented in Lambeck and others (2002). Relatively rapid sea-level rise associated with meltwater pulse 1A occurred just prior to the minimum age estimate for abandonment of terrace t_2 at ~13.9 ka.

size and color change. Unit 2 consists of 3 to 4 m of regularly alternating, bluish-gray mud or silt draped over medium to fine sands with typical thicknesses of 15 to 25 cm (fig. 3*D*). The sands are well-sorted, clean, and devoid of any sedimentary structures, while the silts are clean, homogeneous, and lack any biogenic material (for example, diatoms, pollen, and organic detritus). We interpret unit 2 as a low-energy, shallow or protected marine facies. The lack of biologic activity may be related to high sedimentation rates, or an unfavorable environment for growth. Unit 2 thickens significantly toward the north in section A, where it contains abundant shell fossils and is interbedded with coarser sands, possibly correlative with the overlying unit 3.

Unit 2 has a transitional contact with unit 3 characterized by increasing sand content and a change in color. We chose a prominent layer with mud rip-up clasts incorporated into an overlying sand layer as the boundary between the units (fig. 3*E*). Unit 3 consists of 9-10 m of tan to light reddish brown coarse sands in shallowly to moderate dipping cross-beds with wavelengths of several meters. Mud drapes (fig. 3*F*), organic-rich layers, concentrations of heavy minerals, and, rarely, very coarse sand to granular layers were all present within the cross-stratification. The presence of heavy mineral sands and low truncation angles to foresets suggests cross bedding in unit 3 is related to wave-base bedforms (White and Williams, 1967). We interpret unit 3 as a shallow marine,

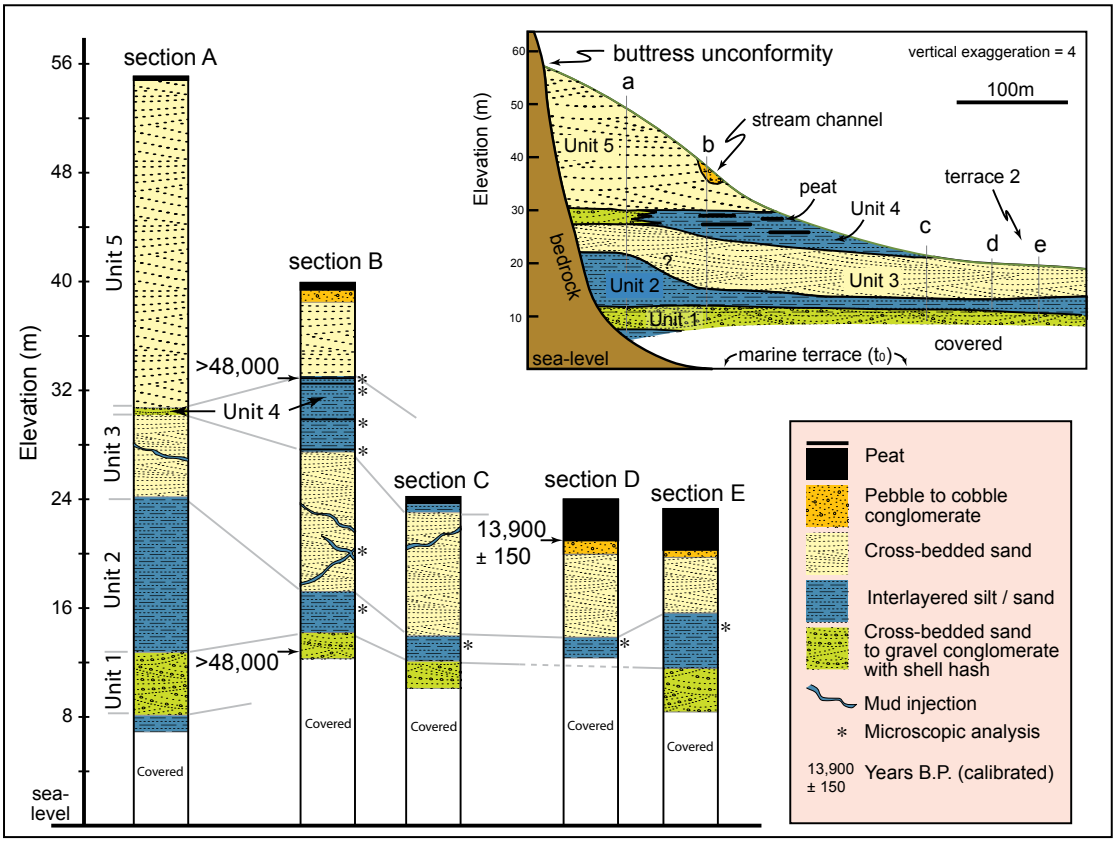

Figure 5. Spatial correlation of measured sections A-E and units 1-5 in the Wingham Island deposits.

Table 1. Radiocarbon dates for selected samples.

[Accelerator Mass Spectrometry ^{14}C ages were obtained by Beta Analytic and calibrated with IntCal04. Calibrated ages are reported to two standard deviations]

Sample	Laboratory No.	Material	$\delta^{13}C$	Conventional ^{14}C Age	Calibrated ^{14}C Age
WingRC18	Beta-239246	peat	-26.9 ‰	12,040 ± 60 B.P.	14,050-13,750 B.P.
WingRC03	Beta-242794	peat	-----	>48,000 B.P.	-----
WingRC01	Beta	wood	-----	>48,000 B.P.	-----

nearshore facies. Multiple generations of mud injections cut through unit 3, in some instances with 20 to 30 cm offset (fig. 3*F*). We suggest these are seismites related to the faults within unit 1 and with a sediment source in unit 2.

Unit 4 consists of ~5 m of alternating light to medium gray silts and sands with thin peat layers (5-20 cm; fig. 3*G*) that were too old for radiocarbon dating (>48 ka; table 1). Unit 4 is in sharp depositional contact with the underlying unit 3. Silts within unit 4 contain abundant organic fragments, although no biological material is present apart from a few bisaccate pollen grains (likely P*inus*), which could be contamination. In section A, the sands and silts are replaced with coarser sands, granular conglomerate and shell hash similar to that in unit 1. This transition represents a lateral facies change towards the buttress unconformity. The top of unit 4 contains well-laminated and regularly alternating thin sand and silt layers that we interpret as rhythmites, which, along with the presence of peat, suggests a tidal to estuarine facies.

Conformably overlying unit 4 is >8 m of medium, well-sorted, tan to light brown, cross-stratified sand of unit 5. Cross-beds are at a high angle to bedding, climb considerably toward the buttress unconformity forming a ~20 m high sand pile-up, and have very fine laminae of heavy minerals on forsets (fig. 3*H*), all suggestive of aeolian processes (White and Williams, 1967). We interpret unit 5 as a beach ridge or dune complex. Channelized lenses of rounded pebble to cobble conglomerate are locally present in the uppermost section of unit 5 (section B, fig. 5), which we interpret as immature fluvial deposits.

Gravel to pebble conglomerate is also present at the top of Sections D and E, where they are in erosional contact with unit 4 (fig. 5). We interpret these occurrences as lag deposits formed following the incision that created terrace t_2. These lag deposits may have been deposited synchronously with the channelized conglomerates in unit 5. Overlying all the measured sections are thick (0.5-3 m) layers of peat, whose deposition post-dates the formation of terrace t_2. A sample from the base of these peat layers in section D yielded a radiocarbon date of 13,900 ± 150 yr B.P. (table 1). This is a minimum age estimate for the formation of terrace t_2, which along with the stratigraphic relationship, constrains the position of sea level at this time.

Sea-Level History

Based on our interpretation of the origin of terrace t_2, RSL was ~20 m higher than present at 13.9 ka. During this time period, RSL was affected by the competing effects of global eustatic sea-level rise and local isostatic rebound following glacial retreat at the end of the LGM. Eustatic sea-level data suggest that sea level has risen 80 to 105 m since 13.9 ka (Lambeck and others, 2002; fig. 4), which, like the age estimate, is a minimum. Because the t_2 surface is ~20 m above modern sea level, we calculate the minimum total surface displacement since 13.9 ka as 100 to 125 m. Furthermore, we suggest that MWP1A may have resulted in a brief period where eustatic sea-level rise kept pace with isostatic uplift, providing the necessary time for the incision of terrace t_2.

Isostatic Uplift

To assess the magnitude and rate of isostatic uplift we apply a 2-dimensional (2D) analytical model of a single, rectangular ice load. Two-dimensional approximations are routinely applied for large ice sheets within a stable continental interior (Greve, 2001). However, in a tectonically active and glacially dynamic area like southern Alaska, this may not be valid. We emphasize that the models presented below are intended to illustrate the general effects of isostatic rebound, but we also attempted to model the crustal response as accurately as possible.

The response of the lithosphere following removal of a glacial load is related to asthenospheric flow and to the elastic strength of the lithosphere. In the case of instantaneous removal of the glacial load (herein referred to as the "flow" model), isostatic uplift is related to the viscosity of the Earth's mantle by

$$w(t) = w_{\max} e^{(-t/t_r)}, \qquad (1)$$

where $w(t)$ is surface displacement remaining until equilibrium with respect to time (t), w_{max} is the total surface displacement, and t_r is the characteristic relaxation time defined as

$$t_r = \frac{4\pi}{\rho_m g \lambda} \quad , \tag{2}$$

where μ is the upper mantle viscosity, ρ_m is the density of the upper mantle, g is the gravitational constant, and λ is the wavelength of the glacial load (table 2; Turcotte and Schubert, 2002). The surface displacement, $w(t)$, represents the amount of isostatic uplift remaining until equilibrium and decreases exponentially such that $w(t=0) = w_{max}$. The uplift rate is the derivative of equation 1 with respect to time.

We chose an average upper mantle viscosity of 2×10^{19} Pa•s, based on glacial-rebound studies in Glacier Bay that suggest viscosities ranging from 3.7×10^{18} to 5×10^{19} Pa•s. (Larsen and others 2003; 2004; 2005). This is consistent with values elsewhere along the southeastern Alaska and British Columbia margin (Clague and James, 2002), but it is low compared to other regions like the Canadian Shield and Northern Europe that have mantle viscosities of 10^{20} to 10^{22} Pa•s (Mitrovica and Peltier, 1992; Lambeck and others, 1990). The wavelength of the glacial load was based on the distance from the glacial divide in the St. Elias Mountains to the LGM extent offshore (~150 km; table 2).

Previous to this study, there were no explicit estimates of the total surface displacement in the study area as a result of glacial loading in the LGM. If we make the simplifying assumption that net tectonic uplift is negligible, glacioisostatic adjustment is equal to the total crustal displacement (w_{max}), calculated in the previous section as 100 to 125 m (table 2). Because isostatic equilibrium is achieved relatively quickly (<5 k.y.; Larsen and others, 2005), we can estimate total ice thickness (h) at the height of the LGM by using Archimedes' principle

$$h = w_{\max} \frac{\rho_m}{\rho_i} \quad , \tag{3}$$

where ρ_i is density of ice, suggesting an ice thickness of 350 to 450 m. Although the Wingham Island deposits are presently above sea-level, they are surrounded by an erosional LGM surface that is now underwater and depressed by the overlying weight of the water and young sediments so that an ice thickness of 350 to 450 is an underestimate. Expanding equation 3 to include these factors yields

$$h = \frac{w_{\max}\rho_m + \rho_w t_w + \rho_s t_s}{\rho_i} \quad , \tag{4}$$

where ρ_w and ρ_s are the density of water and sediment, respectively, t_w is the average water depth, and t_s is the thickness of post-LGM sediments as determined from Jaeger and others (1998) and Worthington and others (2008; table 2). This suggests an upper limit for ice thickness of 600 to 700 m, which brackets the estimated ice thickness along the British Columbia coast during the LGM (Hetherington and others, 2004).

Combining total surface displacement, w_{max}, in equations 1 and 2, we calculate isostatic uplift as a function of time following deglaciation (fig. 6*A*). Postglacial rebound is initially rapid, with rates exceeding 10 cm/yr for the first few hundred years, and remains above 1 cm/yr for nearly 3,000 yr (fig. 6*A*). Similarly high rates of initial postglacial rebound have been estimated for Puget Sound (~40 cm/yr) (Dethier and others, 1995), along the British Columbia coast (>10 cm/yr) (Clague and James, 2002), and Glacier Bay where modern uplift rates are 3 to 4 cm/yr in response to the end of the last pulse of the Little Ice Age about 100 years ago (Larsen and others, 2003; 2005).

Because the "flow" model assumes instantaneous ice removal, which may be a poor assumption, we also calculated isostatic rebound in response to a retreating ice sheet by modeling the elastic flexure of the lithosphere overlying a fluid half-space (herein referred to as the "flexure" model). Assuming the foredeep in front of the retreating ice sheet is filled with water of density ρ_w, the surface displacement, $w(x)$ with respect to the horizontal position (x) from the center of the load, is given by

$$w(x) = \frac{\rho_i h}{2(\rho_m - \rho_w)}\left[2 - e^{\left(\frac{-x+\lambda}{\alpha}\right)}\cos\left(\frac{x+\lambda}{\alpha}\right) - e^{\left(\frac{-\lambda+x}{\alpha}\right)}\cos\left(\frac{\lambda-x}{\alpha}\right)\right], \tag{5A}$$

when $x < \lambda$, and by

$$w(x) = \frac{\rho_i h}{2(\rho_m - \rho_w)}\left[e^{\left(\frac{-x-\lambda}{\alpha}\right)}\cos\left(\frac{x-\lambda}{\alpha}\right) - e^{\left(\frac{\lambda-\chi}{\alpha}\right)}\cos\left(\frac{\lambda+x}{\alpha}\right)\right], \tag{5B}$$

when $x > \lambda$, (Angevine and others, 1990). In equations 5*A* and 5*B*, α is the flexural parameter, which is given by

$$\alpha = \sqrt[4]{\frac{T_e E}{3\rho_m g\,(1-\nu^2)}} \quad , \tag{6}$$

where T_e is the effective elastic thickness of the lithosphere, E is Young's modulus, and ν is Poisson's ratio (table 2). We use an elastic thickness of 15 km based on refraction and seismic inversion studies near Wingham Island that image the Moho (Eberhart-Phillips and others, 2006; Brocher and others, 1994).

The "flexure" model is presented in figure 6*B* where the range in values of surface displacement (green shaded area) represents the uncertainty associated with crustal depression and ice thickness. Because the amount of surface displacement in this approach is dependent on the distance from the ice front, we calculated surface displacement in time (fig. 6*B*) by using the distance between Wingham Island and various onshore points for which there are timing constraints of glacial retreat. We also include the general ages of 15.5 ± 1 ka constraint for the beginning of glacial retreat and 9 ± 1 ka constraint for the completion of glacial retreat based on regional patterns (Clague and James, 2002). In the Katalla Bay area, we prefer the older deglaciation age of ~14.5 ka (Sirkin and Tuthill, 1987;

Table 2. Variable used in equations.

Symbol	Description	Value	Reference or Note
α	flexural parameter	~40 km	calculated
E	Young's modulus	7×10^{10} Pa	Turcotte and Schubert (2002)
g	gravitational acceleration	9.81 m/s^2	
h	ice thickness	650 +/- 50 m	calculated
λ	½ wavelength for load	75 km	½ distance to drainage divide
μ	viscosity	2×10^{19} Pa•s	Larsen and others (2003; 2004; 2005)
ρ_i	density ice	930 kg/m^3	
ρ_m	density upper mantle	3,300 kg/m^3	
ρ_s	density sediment	2,200 kg/m^3	
ρ_w	density water	1,000 kg/m^3	
T_e	elastic thickness	15 km	Eberhart-Phillips and others (2006)
t_r	relaxation time	1,230 yr	calculated
t_s	sediment thickness	100 m	Jaeger and others (1998)
t_w	water depth	15 m	USGS topographic maps
v	Poisson's ratio	0.25	Turcotte and Schubert (2002)

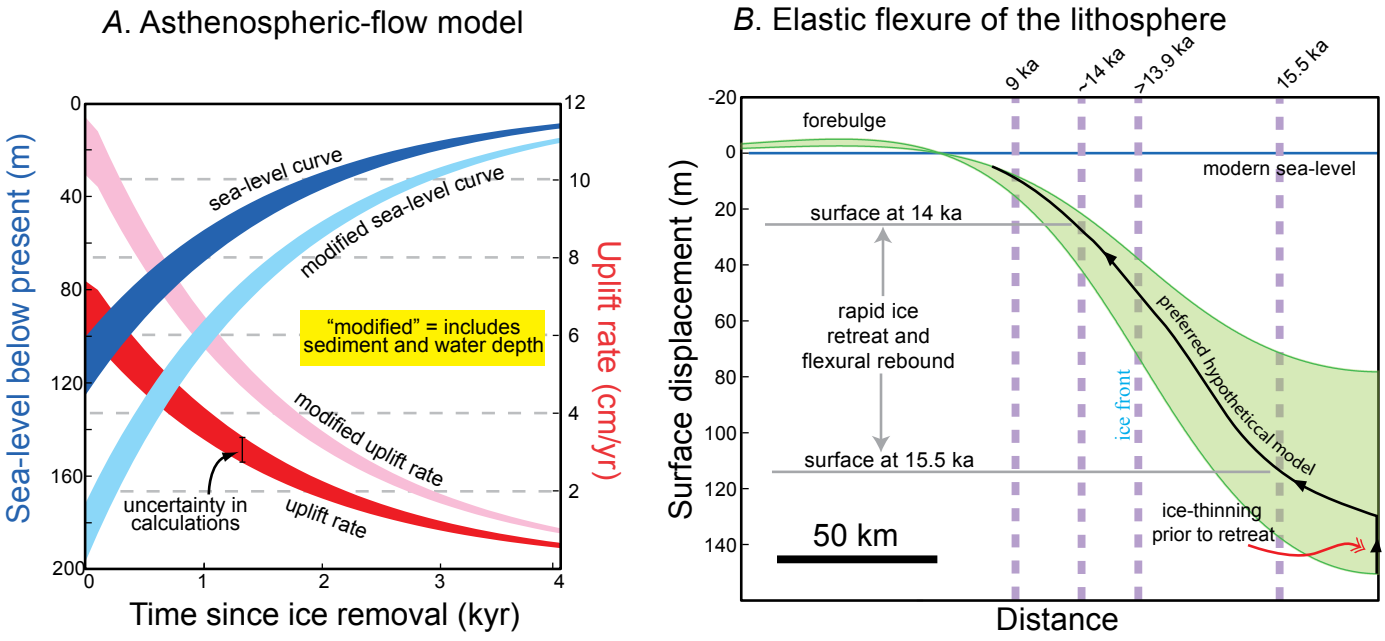

Figure 6. *A*, The asthenospheric "flow" model for isostatic adjustment showing an increasing cumulative surface displacement and decreasing uplift rate as a function of time since instantaneous removal of the glacial load (at t=0). The "modified" curves include sediment accumulation since the last Glacial maximum and present water depth, which we consider more accurate (equation 4). Initial uplift rates exceed 10 cm/yr and 66 percent of isostatic rebound is completed within 2 k.y. *B*, The "flexure" model of isostatic rebound assuming bending of a thin elastic plate over an incompressible fluid half-space. The model predicts a ~5 m high forebulge in front of the glacial load. The position of the ice front at varying times is plotted (dashed purple vertical lines) and used to constrain the timing of isostatic uplift in response to flexure of the lithosphere as ice retreats (fig. 7). In general, ice retreat is very rapid following the beginning of deglaciation. In both *A* and *B* the shaded areas represent uncertainty associated with total crustal displacement and ice thickness.

fig. 1), although the young ages (~9.5-10 ka; labeled as a possible glacial readvance in fig. 7) are also included for comparison (Huesser, 1960; Fleisher and others, 1999).

Glacial thinning is likely to occur prior to ice retreat resulting in restrained rebound (Benn and Evans, 1998). For the Laurentide ice sheet, Andrews (1973) suggested up to 75 percent of total rebound may be restrained, which we consider a maximum value. Restrained rebound in the Cordilleran Ice Sheet is unlikely because tidewater glaciers are keenly sensitive to sea level rise, which often results in rapid rates of retreat due to calving (Clague and James, 2002). The black arrows in figure 6*B* represent a modest 15 percent restrained rebound and are intended to illustrate a possible path of crustal displacement during glacial retreat. Although our error calculations remain unchanged, we use the 15 percent restrained rebound curve for a centroid in figure 7.

Discussion and Conclusions

The two models ("flexure" and "flow") are plotted with the eustatic sea-level curve in figure 7. The flexure model is tied to the sea-level curve based on the onshore age data, but the only control points for the "flow" model are the time of instantaneous ice removal and the age of abandonment for terrace t_2. In general, the two models compare well because ice retreat was sufficiently rapid following deglaciation to meet the instantaneous load removal assumption in the "flow" model. The uplift rates for the first thousand years are actually greater for the "flexure" model than the predicted rates for the "flow" model, suggesting isostatic rebound may initially be limited by the viscosity of the upper mantle if both processes simultaneously affect rebound. After a period of rapid retreat, stabilized glacial systems onshore may begin

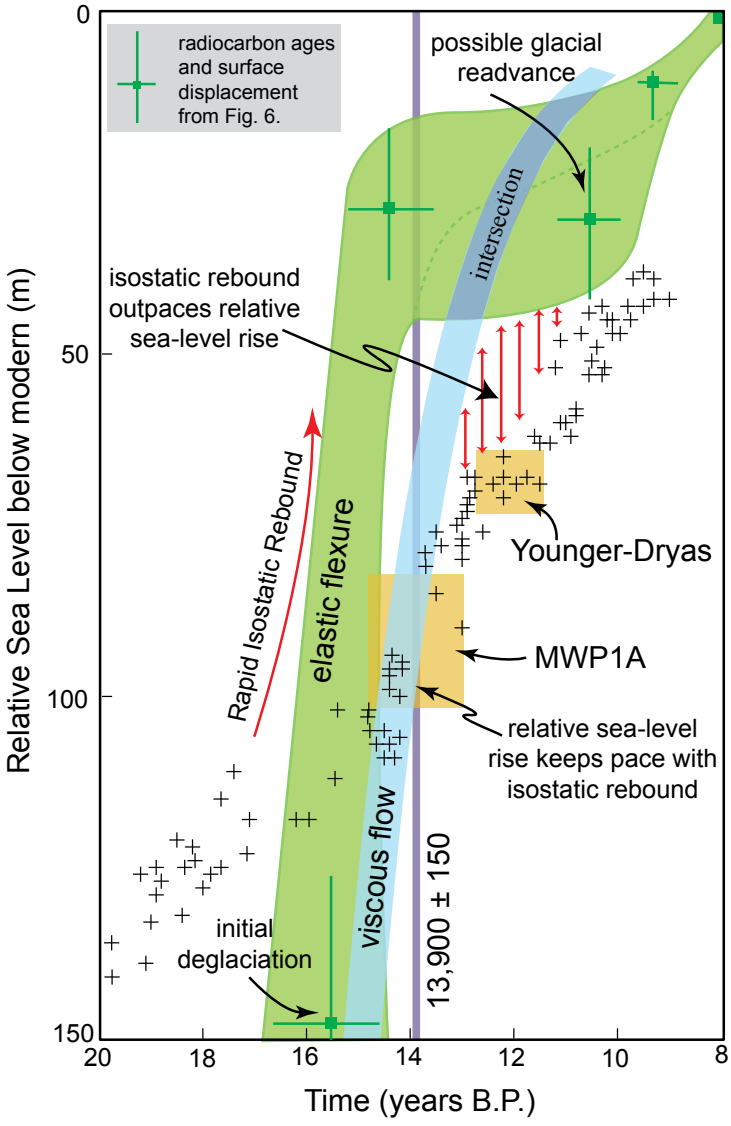

Figure 7. The relative sea-level (RSL) curves predicted by the two isostatic ("flow" and "flexure") models from fig. 6, combined with eustatic sea-level data (black crosses) from figure 4. The rate of sea-level rise associated with meltwater pulse 1A (MWP1A) is close to the rate of isostatic uplift in both the "flow" and "flexure" models. Rapid ice retreat suggests that initial isostatic rebound was largely, if not entirely, limited by the viscosity of the asthenosphere. The intersection of the "flow" and "flexure" models curves may represent the time after which the rate of isostatic rebound was limited by the collapse of a foredeep in front of the retreating ice.

to limit rebound (represented by the area of intersection in figure 7). Thus, during glacial retreat, a transition may occur in the dominant mode of isostatic response.

Both models show that isostatic rebound outpaced sea level rise during the last 11 to 15 k.y. The only period where the rate of sea-level rise approaches the rates of isostatic uplift predicted in either the "flow" or "flexure" model, was during MWP1A, which is consistent with the timing for the abandonment of terrace t_2. In this scenario, the temporary lull in RSL fall provided the time necessary to stabilize sea-level and incise t_2. A rise in RSL can also occur during the collapse of a glacial forebulge as documented in the Queen Charlotte Islands to the southeast (Luternauer and others, 1989; Hetherington and others, 2004). In these studies, the existence and migration of a forebulge resulted in local uplift (lowering RSL) and emergence above sea level, followed by forebulge collapse (raising RSL) and continued eustatic sea level rise, such that the emergent deposits (terrestrial facies) are now submerged 80 to 100m below modern sea level. The collapse of the forebulge is one of the final stages in the rebound process and only small, isostatic adjustments from glacial unloading are expected to occur after the forebulge has migrated or collapsed. The "flexure" model predicts a small, ~5 m forebulge located 75 to 100 km from the ice front, suggesting ~5 m of RSL rise in response to forebulge collapse (fig. 6*B*). Because little isostatic uplift is expected following forebulge collapse, absolute sea level would need to have been close (~5 m) to its present position at ~13.9 ka, which is clearly not the case as documented by terrace t_2 that is presently ~20 m above sea level.

There is theoretical evidence that viscous flow in the deep mantle may influence the isostatic response at long wavelengths, whereas flow in the upper mantle controls short wavelength isostatic perturbations (Mitrovica and Peltier, 1991). This could suggest that the response to rapid retreat of glacial ice and an associated migration or collapse of a forebulge, controlled by upper mantle flow, may be superimposed on a broader, regional isostatic-uplift signal, controlled by deep mantle flow. In this case, the timing for forebulge collapse may not occur during the final stages of isostatic rebound. However, we have no way to distinguish between the effects or timing of a transient forebulge and more general isostatic uplift controlled by the deep mantle. In lieu of more data, we prefer the simpler explanation that the lull in RSL fall causing the incision of terrace t_2 is related to MWP1A rather than a superimposed isostatic response.

The timing of ice retreat and emergence of Wingham Island have important implications for the early migration of humans into North America. Our results show that by ~13.9 ka, the Cordilleran Ice Sheet had retreated past Wingham Island, and rapid uplift had resulted in a emergent paleoshoreline. Based on the modeled rates of isostatic rebound, Wingham and Kayak Island were likely connected to the mainland by a land bridge within a thousand years of their emergence. While isostatic uplift exceeded eustatic sea level rise (until ~ 11 ka, fig. 7), RSL continued to fall, exposing portions of the continental shelf that may have been suitable for human occupation or travel. Unlike areas along the British Columbia coast that were resubmerged by ~9.5 ka (Josenhans and others, 1997), the Wingham Island area remained above sea level to the present. These conclusions are consistent with a coastal migration route for early humans into the Americas (Fladmark, 1979) and can help explain the presence of pre-Clovis artifacts, remains, and coprolites along the western seaboard (Dillehay, 1997; Dixon, 2001; Goebel and others, 2008).

Acknowledgments

This research was supported by NSF grant EAR0409009 to T. Pavlis. Reviews by Jose Hurtado and Tom Hamilton improved the paper. Ken Ridgway and Richard Langford provided valuable discussion of depositional environments. William Cornell kindly assisted our efforts with micropaleontological analysis.

References Cited

Andrews, J.T., 1973, The Wisconsin Laurentide Ice Sheet—dispersal centers, problems of rates of retreat, and climatic implications: Arctic and Alpine Research, v. 5, p. 185–199.

Angevine, C.L., Heller, P.L., and Paola, C., 1990, Quantitative sedimentary basin modeling: A.A.P.G. Continuing Education Course Note Series 32, 133 p.

Bard, E., Hamelin, B., Arnold, M., Montaggioni, L., Cabioch, G., Faure, G., and Rougerie, F., 1996, Deglacial sea-level record from Tahiti corals and the timing of global meltwater discharge: Nature, v. 382, p. 241–244.

Bard, E., Hamelin, B., and Fairbanks, R.G., 1990, U/Th ages obtained by mass spectrometry in corals from Barbados, sea level during the past 130,000 years: Nature, v. 346, p. 456–458.

Benn, D.I., and Evans, D.J.A., 1998, Glaciers and glaciation: New York, Wiley, 734 p.

Blaise, B., Clague, J.J., and Mathewes, R.W., 1990, Time of maximum Late Wisconsin glaciation, west coast of Canada: Quaternary Research, v. 34, p. 282–295.

Blanchon, P., and Shaw, J., 1995, Reef drowning during the last deglaciation—Evidence for catastrophic sea-level rise and ice-sheet collapse: Geology v. 23, p. 4–8.

Booth, D.B., Troost, K.G., Clague, J.J., and Waitt, R.B., 2004, The Cordilleran ice sheet: Developments in Quaternary Science, v. 1, p. 17–43.

Brocher, T.M., Fuis, G.S., Fisher, M.A., Plafker, G., and Moses, M.J., 1994, Mapping the megathrust beneath the northern Gulf of Alaska using wide-angle seismic data: Journal of Geophysical Research, v. 99, p. 11663–11685.

Calkin, P.E., Wiles, G.C., and Barclay, D.J., 2001, Holocene coastal glaciation of Alaska: Quaternary Science Review: v. 20, p. 449–461.

Carlson, P.R., Bruns, T.R., and Fisher, M.A., 1990, Development of slope valleys in the glacimarine environment of a complex subduction zone, Northern Gulf of Alaska, *in* Dowdeswell, J. A., and Scourse, J.D., eds., Glacimarine environments—Processes and sediments: Geological Society Special Publication, p. 39–153.

Chapman, J.B., and Vorkink, M., 2006, Tectonic geomorphology in an orogen dominated by glacial erosion, Saint Elias Mountains, Alaska, [abs.]: American Geophysical Union Chapman conference on active tectonics and seismic potential of Alaska, Girdwood, Alaska.

Clague, J.J., and James, T.S., 2002, History and isostatic effects of the last ice sheet in southern British Columbia: Quaternary Science Reviews, v. 21, p. 71–87.

Clark, P.U., and Mix, A.C., 2002, Ice sheets and sea level of the last glacial maximum: Quaternary Science Reviews, v. 21, p. 1–7.

Cohen, S.C., and Freymueller, J.T., 2005, Crustal deformation in southcentral Alaska: The 1964 Prince William Sound Earthquake Subduction Zone: Advances in Geophysics, v. 47.

Denton, G.H., 1974, Quaternary glaciations of the White River valley, Alaska, with a regional synthesis for the northern St. Elias mountains, Alaska and Yukon Territory: Geological Society of America Bulletin, v. 85, p. 871–892.

Dethier, D.P., Pessel, F., Jr., Keuler, R.F., Balzarini, M.A., and Pevear, D.R., 1995, Late Wisconsinan glaciomarine deposition and isostatic rebound, Northern Puget Lowland, Washington: Geological Society of America Bulletin, v. 107, p. 1288–1303.

Dillehay, T., 1997, Monte Verde: A Late Pleistocene site in Chile, Vol. 2: The archaeological context and interpretation: Washington, D.C., Smithsonian Institution Press.

Dixon, E.J., 2002, How and when did people first come to North America?: Athena Review, v. 3, no. 2, p. 23–27.

Dixon, E.J., 2001, Human colonization of the Americas—timing, technology, and process: Quaternary Science Reviews, v. 20, p. 277–299.

Eberhart-Phillips, D., Christensen, D.H., Brocher, T.M., Hansen, R., Ruppert, N.A, Haeussler, P.J., and Abers, G.A., 2006, Imaging the transition from Aleutian subduction to Yakutat collision in central Alaska, with local earthquakes and active source data: Journal of Geophysical Ressearch, v. 111, B11303, doi:10.1029/2005JB004240.

Eyles, C.H., Eyles, N., and Lagoe, M.B., 1991, The Yakataga Formation, a late Miocene to Pleistocene record of temperate glacial marine sedimentation in the Gulf of Alaska, *in* Anderson, J.B. and Ashley, G.M., eds., Glacial-marine sedimentation, paleoclimatic significance: Geological Society of America Special Paper, v. 261, p. 159–180.

Fairbanks, R.G., 1989, A 17,000-year glacio-eustatic sea level record—influence of glacial melting dates on the Younger Dryas event and deep ocean circulation: Nature v. 342, p. 637–642.

Fladmark, K.R., 1979, Routes—Alternate migration corridors for early man in North America: American Antiquity, v. 44, p. 55–69.

Fleisher, P.J., Muller, E.H., Peteet, D.M., and Lachniet, M.S., 1999, Arctic enigma: Geotimes, v. 44, no. 1, p.16–21.

Goebel, T., Waters, M.R., O'Rourke, D.H., 2008, The Late Pleistocene dispersal of modern humans in the Americas: Science, v. 319, p. 1497–1501.

Gorham, E., Lehman, C., Dyke, A., Janssens, J., and Dyke, L., 2007, Temporal and spatial aspects of peatland initiation following deglaciation in North America: Quaternary Science Reviews, v. 26, p. 300–311.

Greene, H.G., Bizzarro, J.J., O'Connell, V.M., and Brylinsky, C.K., 2007, Construction of digital potential marine benthic habitat maps using a coded classification scheme and its application, *in* Todd, B.J., and Greene, H.G., eds., Mapping the Seafloor for Habitat Characterization: Geological Association of Canada, Special Paper 47, p. 141–155.

Greve, R., 2001, Glacial isostasy—Models for the response of the Earth to varying ice loads, *in* Straughan, B., Greve, R., Ehrentraut, H., and Wang, Y., eds, Continuum mechanics and applications in geophysics and the environment: New York, Springer, p. 307–325.

Hamilton, S., and Shennan, I., 2005a, Late Holocene great earthquakes and relative sea-level change at Kenai, southern Alaska: Journal of Quaternary Science., v. 20, no. 2, p. 95–111.

Hamilton, S., and Shennan, I., 2005b, Late Holocene relative sea-level changes and the earthquake deformation cycle around upper Cook Inlet, Alaska: Quaternary Science Review, v. 24, p. 1479–1498.

Hamilton, T.D., 1994, Late Cenozoic glaciation of Alaska, *in* Plafker, G., and Berg, H.C., eds., The geology of Alaska: The Geology of North America: Geological Society of America, v. G-1, p. 813–844.

Hanebuth, T., Stattegger, K., and Grootes, P., 2000, Rapid flooding of the Sunda Shelf—a late glacial sea-level record: Science, v. 288, p. 1033–1035.

Hetherington, R., Barrie, J.V., Reid, R.G.B., MacLeod, R., and Smith, D.J., 2004, Paleogeography, glacially induced crustal displacement, and late Quaternary coastlines on the continental shelf of British Columbia, Canada: Quaternary Science Reviews, v. 23, no. 3–4, p. 295–318.

Heusser, C.J., 1960, Late Pleistocene environments of North Pacific North America: American Geographical Society Special Publication, v. 35, 308 p.

Jaeger, J.M., Nitrouer, C.A., Scott, N.D, and Milliman, J.D., 1998, Sediment accumulation along a glacially impacted mountainous coastline—North-east Gulf of Alaska: Basin Research, v. 10, p. 155–173.

Josenhans, H.W., Fedje, D.W., Pienitz, R., and Southon, J., 1997, Early humans and rapidly changing Holocene sea levels in the Queen Charlotte Islands-Hecate Strait, British Columbia, Canada: Science, v. 277, p. 71–74.

Kaufman, D.S., and Manley, W.F., 2004, Pleistocene maximum and Late Wisconsin glacier extents across Alaska, U.S.A., *in* Ehlers, J., and Gibbard, P.L., eds., Quaternary Glaciations—Extent and Chronology, Part II, North

America: Elsevier, Developments in Quaternary Science, v. 2b, p. 9–27.
Lambeck, K., and Chappell, J., 2001, Sea-level change through the last glacial cycle: Science, v. 292, p. 679–686.
Lambeck, K., Johnson, P., and Nakada, M., 1990, Holocene glacial rebound and sea-level change in NW Europe: Geophysics Journal International, v. 103, p. 451–468.
Lambeck, K., Yokoyama, Y., and Purcell, T., 2002, Into and out of the last glacial maximum—sea-level change during oxygen isotope Stages 3 and 2: Quaternary Science Reviews, v. 21, p. 343–360.
Larsen, C.F., Echelmeyer, K.A., Freymueller, J.T., and Motyka, R.J., 2003, Tide gauge records of uplift along the northern Pacific-North American plate boundary, 1937 to 2001: Journal of Geophysical Research, v. 108, p. 2216.
Larsen, C.F., Motyka, R.J., Freymueller, J.T., Echelmeyer, K.A., and Ivins, E.R., 2005, Rapid viscoelastic uplift in southeast Alaska caused by post-Little Ice Age glacial retreat: Earth and Planetary Science Letters v. 23, p. 548–560.
Larsen, C.F., Motyka, R.J., Freymueller, J.T., Echelmeyer, K.A., and Ivins, E.R., 2004, Rapid uplift of southern Alaska caused by recent ice loss: Geophysics Journal International, v. 158, p. 1118–1133.
Luternauer, J.L., Clague, J.J, Conway, K.W., Barrie, J.V., Blaise, B. and Mathewes R.W., 1989, Late Pleistocene terrestrial deposits on the continental shelf of western Canada: Evidence for rapid sea-level change at the end of the last glaciation: Geology, v. 17, p. 357–360.
Mann, D.H., and Hamilton, T.L., 1995. Late Pleistocene and Holocene paleoenvironments of the North Pacific coast: Quaternary Science Reviews, v. 14, p. 449–471.
Messina, C., and Labarbera, M., 2004, Hydrodynamical behavior of brachiopod shells—experimental estimates and field observations: Palaios, v. 19, n. 5, p. 441–450.
Miller, D.J., 1958, Anomalous glacial history of the northeastern Gulf of Alaska Region: Geological Society of America Bulletin, v. 69, p.1613–1614.
Miller, D.J., 1961, Geology of the Katalla district, Gulf of Alaska Territory Province, Alaska; U.S. Geological Survey Open-File Report 61–99, map with text, 2 sheets.
Mitrovica, J.X., and Peltier, W.R., 1992, Constraints on mantle viscosity from relative sea level variations in Hudson Bay: Geophysical Research Letters, v. 19, n. 12, p. 1185–1188.
Mitrovica, J.X., and Peltier, W.R., 1991, A complete formalism for the inversion of post-glacial rebound data—resolving power analysis: Geophysics Journal International, v. 104, p. 267–288.
Muller, E.H., and Fleisher, P.J., 1995, Surging history and potential for renewed retreat—Bering Glacier, Alaska, U.S.A.: Arctic and Alpine Research, v. 27, p.81–88.
Pasch, A., and Foster, N., 2006, What are clams doing in the Bering glacier? [abs.]: Geological Society of America Abstracts with Programs, n. 27–4.
Plafker, G., 1969, Tectonics of the March 27, 1964, Alaska earthquake: U.S. Geological Survey Professional Paper 543-I, 74 p.
Plafker, G., 1974, Preliminary geologic map of Kayak and Wingham Islands, Alaska: U. S. Geological Survey, Open-File Report: OF 74-0082, 1 sheet.
Plafker, G., 1987, Regional geology and petroleum potential of the northern Gulf of Alaska, *in* Scholle, D.W., Grantz, A., and Vedder, J.G., eds., Geology and resource potential of the continental margin of the western North American and adjacent ocean basins—Beaufort Sea to Baja California: Circum-Pacific Council for Energy and Mineral Resources, Earth Science Series, v. 6, p. 229–268.
Plafker, G., Lajoie, K.R., and Rubin, M., 1992, Determining intervals of great subduction zone earthquakes in southern Alaska by radiocarbon dating, *in*, Taylor, R.E., Long, A., Kra, R.S., eds., Radiocarbon after four decades—An interdisciplinary perspective: New York, Springer, p. 436–452.
Reid, J.R., 1970, Late Wisconsin and Neoglacial history of the Martin River Glacier, Alaska: Geological Society of America Bulletin, v. 81, p. 3593–3604.
Rymer, M.J., and Sims, J.D., 1982, Lake-sediment evidence for the date of deglaciation of the Hidden Lake area, Kenai Peninsula, Alaska: Geology, v. 10, p. 314–316.
Shennan, I., Scott, D., Rutherford, M., and Zong, Y., 1999, Microfossil analysis of sediments representing the 1964 earthquake, exposed at Girdwood Flats, Alaska, USA: Quaternary International, v. 60, p. 55–73.
Sirkin, L., and Tuthill, S.J., 1987, Late Pleistocene and Holocene deglaciation and environments of the southern Chugach Mountains, Alaska: Geological Society of America Bulletin, v. 99, p. 376–384.
Turcotte, D.L., and Schubert, G., 2002, Geodynamics: New York, Cambrige Univesity Press, , 456 p.
White, J.R., and Williams, E.G., 1967, The nature of fluvial process as defined by settling velocities of heavy and light minerals: Journal of Sedimentary Research, v. 37, n. 2, p. 530–539.
Worthington, L.L., Gulick, S.P., and Pavlis, T.L., 2008, Identifying active structures in the Kayak Island and Pamplona Zone—Implications for offshore tectonics of the Yakutat microplate, Gulf of Alaska, *in*, Freymueller, J.T., Haeussler, P.J., Wesson, R.L., Ekstrom, G., eds., Active Tectonics and Seismic Potential of Alaska: Geophysical Monograph Series, v. 179, p. 257–268.

This page intentionally left blank

This page intentionally left blank

USGS Haeussler and Galloway, editors—**Studies by the U.S. Geological Survey in Alaska, 2007**—Professional Paper 1760–B